

The nuage mediates retrotransposon silencing in mouse primordial ovarian follicles

Ai Khim Lim^{1,*}, Chanchao Lorthongpanich^{1,2,*}, Ting Gang Chew¹, Chin Wee Godwin Tan³, Yan Ting Shue⁴, Sathish Balu¹, Natalia Gounko⁵, Satomi Kuramochi-Miyagawa⁶, Martin M. Matzuk⁷, Shinichiro Chuma⁷, Daniel M. Messerschmidt¹, Davor Solter^{1,9} and Barbara B. Knowles^{1,10}

SUMMARY

Mobilization of endogenous retrotransposons can destabilize the genome, an imminent danger during epigenetic reprogramming of cells in the germline. The P-element-induced wimpy testis (PIWI)-interacting RNA (piRNA) pathway is known to silence retrotransposons in the mouse testes. Several piRNA pathway components localize to the unique, germline structure known as the nuage. In this study, we surveyed mouse ovaries and found, for the first time, transient appearance of nuage-like structures in oocytes of primordial follicles. Mouse vasa homolog (MVH), Piwi-like 2 (PIWIL2/MILI) and tudor domain-containing 9 (TDRD9) are present in these structures, whereas aggregates of germ cell protein with ankyrin repeats, sterile alpha motif and leucine zipper (GASZ) localize separately in the cytoplasm. Retrotransposons are silenced in primordial ovarian follicles, and de-repressed upon reduction of piRNA expression in *Mvh*, *Mili* or *Gasz* mutants. However, these null-mutant females, unlike their male counterparts, are fertile, uncoupling retrotransposon activation from sterility.

KEY WORDS: Nuage, Ovary, Primordial follicles, Retrotransposons, piRNAs, Mouse

INTRODUCTION

Maintaining genome integrity in germ cells is of fundamental importance in ensuring accurate transmission of genetic information throughout generations. During germ cell specification, existing epigenetic marks are erased and new ones laid down to establish totipotency (Smallwood and Kelsey, 2012). Genome-wide DNA demethylation and germ cell-specific reestablishment of repressive marks during this reprogramming process transiently alleviates the epigenetic repression of endogenous transposable elements (TEs), which constitute 46% and 39% of the human and mouse genomes, respectively (Lander et al., 2001; Mouse Genome Sequencing Consortium, 2002). Owing to their capacity for random transposition, TEs can act as insertional mutagens or create genomic lesions when transposing, hence endangering genome integrity (Haig and Kazazian, 2004). Although existing TE insertions have been shown to drive diversity in tissues such as brain and placenta (Chuong et al., 2013; Perrat et al., 2013), their transcription and activity in germ cells must be suppressed. Various mechanisms have evolved as a form of defense to combat them.

In germ cells, a unique electron-dense structure known as the nuage is implicated in retrotransposon repression (Aravin et al., 2009; Lim and Kai, 2007). The nuage, also known as intermitochondrial cement, is a ribonucleoprotein complex that shares similar molecular compositions and appears morphologically identical in different organisms (Eddy, 1976). Intermitochondrial cement, observed among mitochondrial clusters in differentiating germ cells, such as spermatogonia and developing oocytes (Eddy, 1976), forms darkly stained material, which is part of the Balbiani body, which comprises mitochondria and endoplasmic reticulum surrounding a Golgi aggregate (Pepling et al., 2007).

In *Drosophila* ovaries and mouse testes, components localizing to the nuage/intermitochondrial cement mediate retrotransposon silencing by regulating the production of a class of small RNAs, piRNAs (Aravin et al., 2009; Lim and Kai, 2007; Ma et al., 2009; Shoji et al., 2009). piRNAs are small RNAs (24–30 nucleotides long) that are processed in a Dicer-independent pathway from long single-stranded precursor transcripts transcribed from discrete genomic loci (Aravin et al., 2007; Brennecke et al., 2007). They act by maintaining TEs in a repressed, methylated state (Kuramochi-Miyagawa et al., 2008), inducing a closed chromatin structure (Le Thomas et al., 2013) and/or degrading the transcripts via the canonical mRNA degradation machinery (Lim et al., 2009).

In mice, the nuage genes are essential for male fertility; loss-of-function mutations of these genes affect distinct stages of spermatogenesis (Pillai and Chuma, 2012). Studies of the presence and function(s) of nuage in the mouse ovary are limited, yet the reported expression of nuage components in mouse oocytes suggests its functional conservation in ovaries (Chuma et al., 2006; Shoji et al., 2009).

Here, we show that a nuage-like structure first appears transiently in the oocytes of primordial follicles of post-natal ovaries, where we observe robust silencing of retrotransposons and retrotransposon-containing genes. However, de-repression of retrotransposons in *Mvh*-, *Mili*- and *Gasz*-null primordial oocytes does not compromise fertility.

¹Institute of Medical Biology, A*STAR, 8A Biomedical Grove, Immunos, 138648 Singapore.

²Siriraj Center of Excellence for Stem Cell Research (SISR), Faculty of Medicine Siriraj Hospital, Mahidol University, Bangkok, Thailand 10700.

³Department of Biological Sciences, National University of Singapore, 117543 Singapore.

⁴School of Biological Sciences, Nanyang Technological University of Singapore, 637551 Singapore.

⁵Joint-Electron Microscopy Suite, A*STAR, Genome, 138671 Singapore.

⁶Graduate School of Frontier Biosciences, Osaka University, Osaka 565-0871, Japan.

⁷Departments of Pathology and Immunology, Molecular and Cellular Biology, Molecular and Human Genetics, and Pharmacology, and Centers for Drug Discovery and Reproductive Medicine, Baylor College of Medicine, Houston, TX 77030, USA.

⁸Institute for Frontier Medical Sciences, Kyoto University, Kyoto 606-8507, Japan.

⁹Duke-NUS, Graduate Medical School, 169857 Singapore.

¹⁰Department of Biochemistry, National University of Singapore, 117597 Singapore.

*These authors contributed equally to this work

†Author for correspondence (aikhim.lim@imb.a-star.edu.sg)

MATERIALS AND METHODS

Mouse strains

B6.Cg.*Mvh*¹⁰⁹⁸ (Tanaka et al., 2000), B6.Cg.*Mili* (Kuramochi-Miyagawa et al., 2004), B6.Cg.*Gasz*^{tm1Zuk} (Ma et al., 2009) and B6.Cg.*Tdrd9*^{tm1Chuma} (Shoji et al., 2009) were backcrossed for six to ten generations onto a C57BL/6J background. Animal work conformed to the guidelines and regulatory standards of A*STAR's Institutional Animal Care and Use Committee.

Collection of primordial follicles and MII oocytes

For primordial follicles, post-natal day (P)5 ovaries were dissected and punctured in M2 medium (Sigma-Aldrich). Upon puncture, oocytes of primordial follicles were released from the somatic cells, collected manually under the microscope by mouth pipetting and washed with M2 medium prior to use. MII oocytes were collected as described (Lorthongpanich et al., 2008).

Indirect immunofluorescence assays (IFA) and histology

For whole-mount staining, P5 ovaries were fixed (5% paraformaldehyde) and blocked then antibody detection was performed as described (Pepling and Spradling, 1998). For cryosections, embryonic day (E)17.5, P5 and adult gonads were fixed (5% paraformaldehyde) and processed (Yamaguchi et al., 2006) then 10- μ m sections were incubated with relevant primary antibodies [MVH (1:500, Abcam13840), MILI (1:50, Abcam36764), TDRD9 (Shoji et al., 2009), GASZ (Ma et al., 2009), SYCP3 (1:50, Abcam97672), IAP-GAG (1:200, Bryan Cullen, Duke University Medical Center, NC, USA)], and finally with Alexa Fluor 488/594-conjugated secondary antibodies (1:400, Invitrogen). For double labeling, MVH antibody was directly conjugated to Alexa Fluor 488 (Mix-n-Stain CF488A antibody labeling kit, Biotium). Images were acquired using a Zeiss META510 inverted confocal microscope. For IFAs, at least two biological samples were examined and a representative, single confocal section was selected from a z-stack series. Hematoxylin and eosin (H&E) staining was performed on ovary sections (Herrán et al., 2011).

Immuno-electron microscopy

Ovaries were fixed (4% paraformaldehyde in 0.1 M phosphate buffer, pH 7.4) and embedded in LR white resin (Electron Microscopy Sciences). Ultrathin sections were cut and incubated with MVH antibody (Abcam13840), followed by 10-nm gold-conjugated secondary antibody. After post-fixing with 2.5% glutaraldehyde and counterstaining with 7% uranyl acetate and Reynold's lead citrate, images were acquired using a JEM-2200FS microscope.

Co-immunoprecipitation (co-IP) and western blot analysis

Two hundred P5 ovaries were lysed in IP buffer [200 mM NaCl, 50 mM Tris, pH 8.0, 0.05% NP-40, complete protease inhibitor cocktail (Roche), 125 U RNase inhibitor]. The lysate was pre-cleared with rabbit IgG-conjugated Protein-A beads, incubated with anti-MVH-conjugated Protein-A beads and eluted for analysis. Primary antibodies used for western blotting were as described for IFA. ACTIN (1:2000, Abcam8227) was used as control. HRP-conjugated secondary antibodies (1:10,000, Jackson ImmunoResearch) were used for detection.

Quantitative reverse transcription-polymerase chain reaction (qRT-PCR)

Primordial follicles were lysed (TaqMan Gene Expression Cells-to-CT lysis buffer) and genomic DNA was removed with DNaseI. For mRNAs, reverse transcription (RT) was carried out using the High Capacity cDNA Reverse Transcription Kit (Applied Biosystems). For small RNAs, RT was performed using NCode miRNA First-Strand cDNA Synthesis Kit (Invitrogen). A mock reaction, without reverse transcriptase, was prepared for each sample. Pre-amplification was performed with the TaqMan PreAmp Master Mix Kit.

Quantitative PCR (qPCR) was carried out using primer sets (supplementary material Table S1) and respective Universal Probe library using TaqMan Fast Universal PCR Master Mix (Applied Biosystems) for mRNAs, and miScript SYBR Green PCR Kit for small RNAs. For amplification and detection, Applied Biosystems 7900HT Fast Real-time

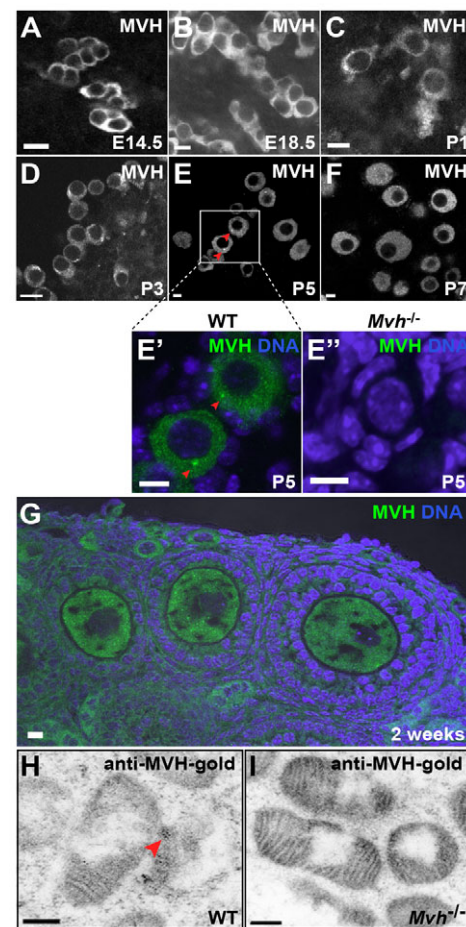


Fig. 1. The nuage is present in primordial follicles of mouse ovaries. (A–G) IFA of MVH in E14.5 (A), E18.5 (B), P1 (C), P3 (D), P5 (E), P7 (F) and 2-week-old (G) wild-type ovaries. MVH aggregates (green; red arrowheads; E') are prominent in the wild-type primordial follicles (P5 ovary) but undetectable in *Mvh* mutants (E''). (H,I) Electron micrographs of immuno-gold-labeled MVH in primordial follicles of P5 wild-type (H) and *Mvh* mutant (I) ovaries. Red arrowhead indicates the MVH-gold labeling at the intermitochondrial cement. Scale bars: 10 μ m (A–G); 200 nm (H,I).

PCR system was used. All results were normalized to *Actb* or *5S rRNA* (*Rn5s* – Mouse Genome Informatics), and fold changes were calculated by normalizing to the endogenous levels. *P*-values were measured using a one-tailed Student's *t*-test.

RESULTS AND DISCUSSION

The nuage is present in the female germline

Several nuage components [MVH (DDX4), TDRD1, TDRD9, mouse PIWI (PIWIL1; also known as MIWI), MILI (PIWIL2) and GASZ] are expressed in mouse oocytes (Chuma et al., 2006; Ding et al., 2013; Shoji et al., 2009; Watanabe et al., 2008; Yan et al., 2002), indicating conservation of the nuage in mouse ovaries. To investigate the presence of nuage-like structure(s), we performed an indirect immunofluorescence assay (IFA) on embryonic, post-natal and adult ovaries. Using antibodies against the well-established nuage marker MVH, we found diffuse staining in the cytoplasm of interconnected cysts in embryonic ovaries (Fig. 1A,B). However, a nuage-like structure was first detected in P1 (Fig. 1C) and P3 (Fig. 1D) ovaries at the onset of cyst

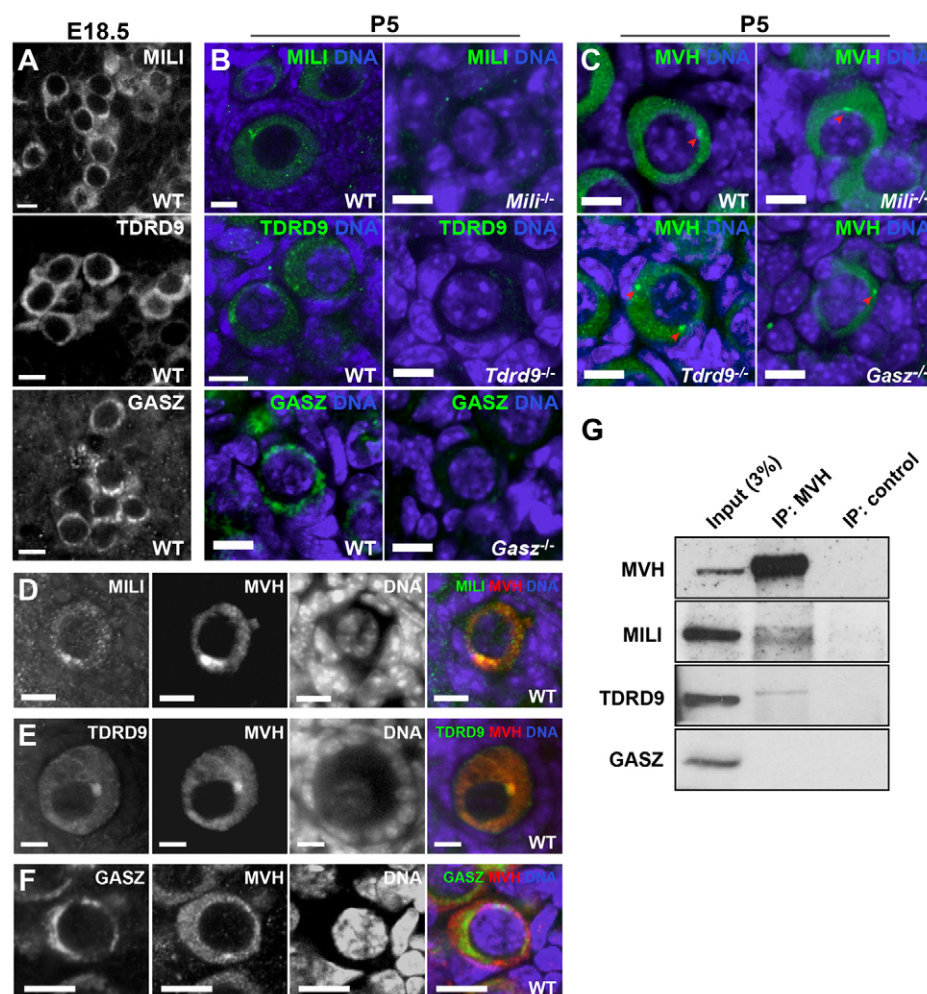


Fig. 2. The nuage is made up of distinct complexes/subcomplexes. (A,B) IFA of nuage proteins, MILI, TDRD9 and GASZ (green in B), in embryonic wild-type (A) and post-natal wild-type and mutant (B) ovaries. (C) IFA of MVH (green) in P5 ovaries of *Mili*, *Tdrd9* and *Gasz* mutants. Red arrowheads indicate the nuage-like aggregates. (D-F) IFA of MILI (green in merge) and MVH (red in merge) (D), TDRD9 (green in merge) and MVH (red in merge) (E), and GASZ (green in merge) and MVH (red in merge) (F) in P5 wild-type ovaries. (G) Western blot of MVH immunoprecipitation in mouse P5 ovarian lysate. Control pull-down was performed with rabbit IgG coupled to Protein-A beads. Scale bars: 10 μ m.

breakdown. These aggregates became more apparent in the primordial follicles on completion of cyst breakdown at P5 (Fig. 1E,E'). Occasionally, MVH-positive aggregates were still detectable in primary follicles (data not shown), but these aggregates diminished in growing and maturing oocytes, and diffuse, cytoplasmic staining was observed (Fig. 1F,G). Importantly, such aggregates were absent in *Mvh*-null primordial follicles, confirming the IFA specificity (Fig. 1E''). Similarly, using immuno-electron microscopy, we detected MVH-gold labeling in the intermitochondrial cement/nuage of wild-type primordial follicles (Fig. 1H; supplementary material Fig. S1C), but not in *Mvh* mutants (Fig. 1I; supplementary material Fig. S1D). In addition, the electron-dense nuage was largely disrupted in *Mvh* mutants (supplementary material Fig. S1A,B) (Chuma et al., 2006).

To confirm the MVH-positive aggregates in primordial follicles, we performed IFA on P5 ovaries using antibodies to MILI and TDRD9, two MVH-interacting proteins in testes (Fig. 2A,B). Both antibodies gave diffuse, cytoplasmic staining in E18.5 gonads, but, like MVH, they localized to nuage-like aggregates in P5 ovaries, which were absent in the respective mutants. GASZ, which is functionally but not structurally linked to the nuage in testes, immunolocalized to cytoplasmic granules in oocytes at E18.5 (Fig. 2A). This granular distribution, which was absent in *Gasz* mutant ovaries, became more intense in wild-type P5 ovaries

(Fig. 2B). To determine whether the nuage structures are present in *Mili*, *Tdrd9* and *Gasz* mutants, we examined MVH localization in P5 mutant ovaries (Fig. 2C). Interestingly, MVH localized to nuage-like aggregates in *Mili*, *Tdrd9* and *Gasz* mutant primordial follicles. However, when performing IFA for MILI in P5 ovaries of *Mvh* mutants, large MILI aggregates were detected (supplementary material Fig. S2), suggesting that organization of the nuage is disrupted.

Co-IFA of P5 ovaries for MILI, TDRD9 or GASZ with MVH confirmed the overlap of MILI and TDRD9 with MVH (Fig. 2D,E); MILI was detected as small, discrete punctate/aggregates within MVH aggregates (Fig. 2D; supplementary material Fig. S2). GASZ staining was distinct from that for MVH, and by inference from TDRD9 and MILI (Fig. 2F). These findings were confirmed biochemically by analyzing MVH immunoprecipitates from P5 ovarian lysates. We found that MILI and TDRD9, but not GASZ, co-immunoprecipitated with MVH (Fig. 2G).

Taken together, our results indicate that the nuage proteins MVH, MILI, TDRD9 and GASZ are found as distinct, transient aggregates in the cytoplasm of primordial ovarian follicles shortly after birth. Human primordial follicles also exhibit transient VASA (DDX4) expression (Castrillon et al., 2000), suggesting that the brief requirement for the nuage is conserved in mammalian germ cells. Intriguingly, the transient appearance of the nuage coincides with that of the Balbiani body (Pepling et al., 2007). The cytoplasmic

arrangement of the organelles into the Balbiani body might facilitate organization of the nuage although the biological implication of this is unknown.

Retrotransposon and endogenous mRNA expression are elevated in the nuage mutants

In mouse testes, MVH, MILI and GASZ repress expression of long interspersed nucleotide element 1 (*LINE1*) and intracisternal A-type particle 1 (*IAP*) retrotransposons (Kuramochi-Miyagawa et al., 2010; Kuramochi-Miyagawa et al., 2008; Ma et al., 2009). To determine whether this function is conserved between the two sexes, we analyzed expression of five retrotransposon families [*LINE1*, *IAP*, mouse transcript (*MT*), murine endogenous retrovirus-like (*MuERV1*) and short interspersed nucleotide element (*SINE*)] in control and *Mvh*, *Mili* or *Gasz* mutant primordial follicles. We found a significant upregulation of all families (Fig. 3A). In addition, IAP-GAG protein, detected by IFA (Fig. 3B) and western blotting (Fig. 3C), was increased in *Mvh*, *Mili* or *Gasz* mutant P5 ovaries. Elevated levels of *LINE1*, *IAP* and *MuERV1* were still detectable in MII oocytes (supplementary material Fig. S3), most likely reflecting transcripts derived from the primordial follicular stage.

Integrated retrotransposon long terminal repeats (LTRs) are often hijacked as alternative promoters, driving and/or coordinating gene expression in oocytes and early embryos (Peaston et al., 2004). To determine whether the nuage mutant-mediated de-repression of retrotransposons also affects expression of chimeric genes, we

assessed expression of three previously described genes: *Dnajc11*, *Glccl1* and *Spin1* (Peaston et al., 2004). Indeed, compared with controls, the expression of all three chimeric genes was elevated in primordial follicles of *Mvh*, *Mili* or *Gasz* mutants (Fig. 3D).

In testes, silencing of retrotransposons requires piRNAs (Pillai and Chuma, 2012). Although piRNA expression has been detected in growing follicles (Watanabe et al., 2008), it was unclear whether piRNAs were required for retrotransposon silencing. We found that piRNAs were greatly reduced in *Mvh*, *Mili* or *Gasz* mutant primordial follicles compared with controls (Fig. 3E). Similarly, two piRNAs on small RNA cluster 4, which target the *MT* retrotransposon (Watanabe et al., 2008) within *Dnajc11*, were reduced in *Mvh*, *Mili* and *Gasz* mutant primordial follicles (Fig. 3F). In *Drosophila*, the nuage proteins generate piRNAs that control embryonic mRNA stability by targeting retrotransposons residing on the 3'UTRs (Rouget et al., 2010). Our data, therefore, reinforce the concept that transposable elements can have a direct developmental function through the nuage and piRNAs.

Retrotransposon de-repression does not lead to sterility in female mice

It was previously shown that pre-pachytene and pachytene piRNAs control retrotransposon repression and meiosis in the mouse testes (Zheng and Wang, 2010). Lack of either class is sufficient to cause meiotic arrest, and nuage-mutant male mice are sterile. Strikingly, *Mvh*, *Mili* and *Gasz* mutant female mice are fertile (Kuramochi-

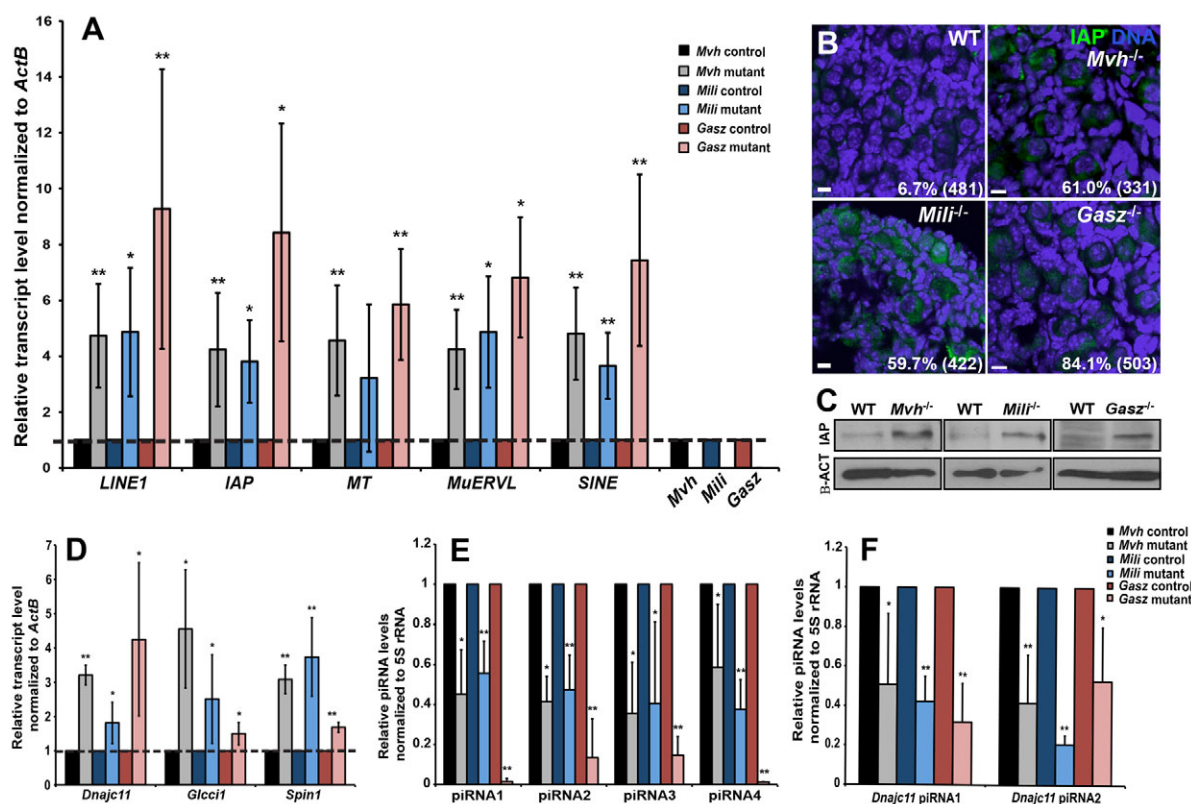


Fig. 3. The nuage genes regulate retrotransposon and endogenous mRNA expression in a piRNA-dependent manner. (A) qRT-PCR of retrotransposons *LINE1*, *IAP*, *MT*, *MuERV1* and *SINE* in *Mvh*, *Mili* and *Gasz* mutant and control primordial follicles. (B) IFA of IAP-GAG (green) in wild-type and *Mvh*, *Mili* and *Gasz* mutant P5 ovaries. Percentage of IAP-positive oocytes (total number of primordial/primary follicles) is indicated. (C) Western blots of IAP-GAG in *Mvh*, *Mili* and *Gasz* mutant P5 ovaries. (D) qRT-PCR of endogenous mRNAs *Dnajc11*, *Glccl1* and *Spin1* in *Mvh*, *Mili* and *Gasz* mutant and control primordial follicles. (E) qRT-PCR of piRNA levels in *Mvh*, *Mili* and *Gasz* mutant and control primordial follicles. (F) qRT-PCR of *Dnajc11* piRNA levels in *Mvh*, *Mili* and *Gasz* mutant and control primordial follicles. * $P < 0.05$, ** $P < 0.01$. Number of biological samples, $n \geq 3$. Error bars represent s.d.

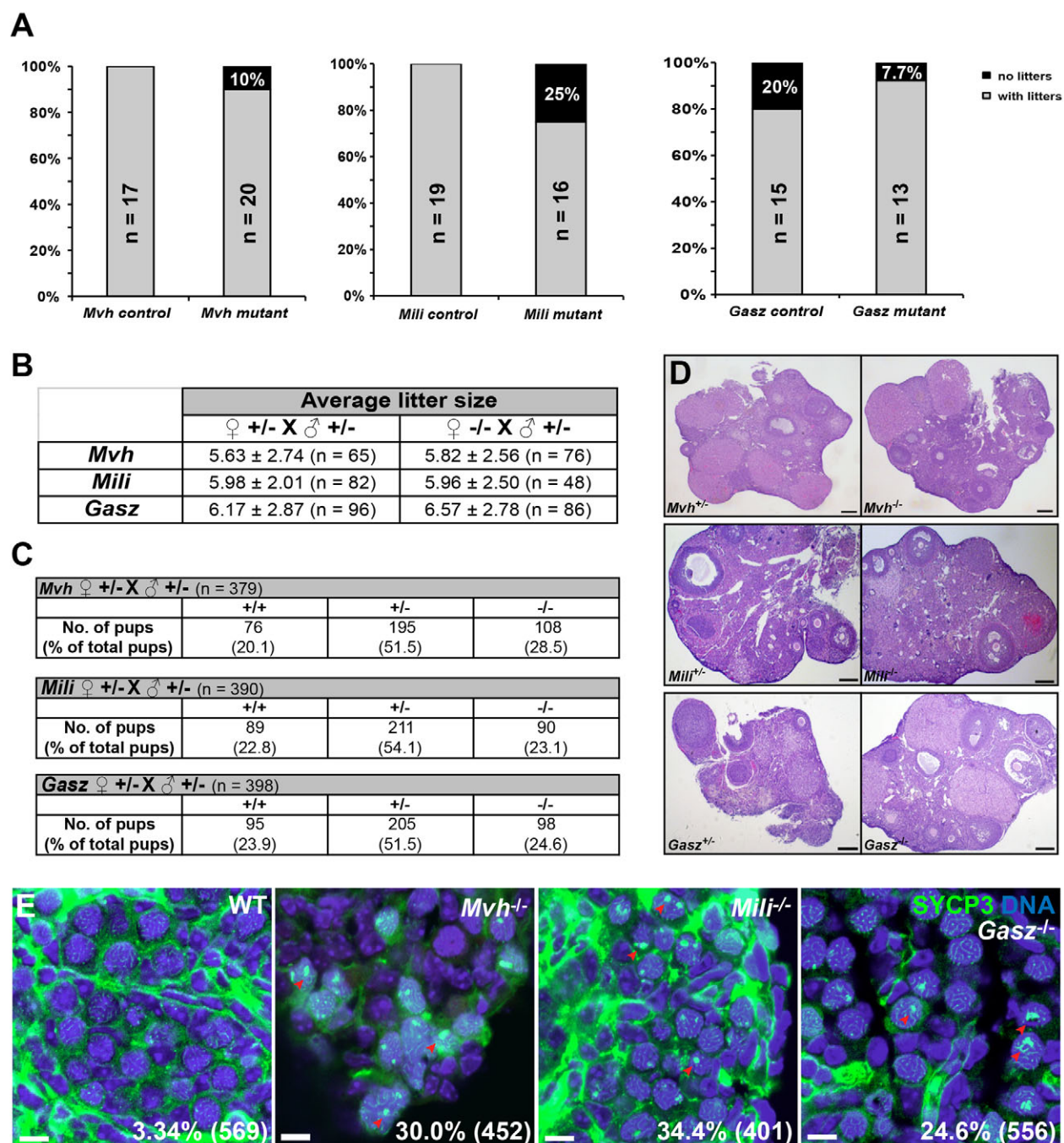


Fig. 4. The nuage mutant females are fertile and exhibit nearly normal oogenesis. (A) Percentages of mutant females that drop litters. Heterozygous males are used for both control (heterozygous female) and mutant (homozygous female) matings. *n*, number of females mated. (B) Average litter size of heterozygous and *Mvh*, *Mili* and *Gasz* mutant females. Average litter size ± s.d. is shown with number of progenies in parentheses. (C) Litters arising from the heterozygous intercrosses indicate a normal Mendelian ratio of 1:2:1. *n*, total number of pups. (D) H&E staining of 10-month-old ovaries from heterozygous and homozygous mutants. (E) Immunostaining of SYCP3 (green) in *Mvh*, *Mili* and *Gasz* E17.5 mutant female gonads. Some mutant oocytes exhibit failure in chromosomal synapsis (red arrowheads). Percentage of oocytes showing asynapsis is shown with total number of oocytes in parentheses. Scale bars: 10 µm.

Miyagawa et al., 2004; Ma et al., 2009; Tanaka et al., 2000), even though we observed ectopic retrotransposon activation in their primordial follicles. As mixed genetic backgrounds in mouse models can veil phenotypic penetrance, we backcrossed *Mvh*, *Mili* and *Gasz* mouse strains onto a C57BL/6J background. The fertility of the mutant females was not significantly different, with regard to

litter frequency or litter size, from controls (Fig. 4A,B). Litters from *Mvh*, *Mili* and *Gasz* heterozygous intercrosses displayed the expected Mendelian ratio of 1:2:1 (wild type, heterozygous, homozygous; Fig. 4C). In tissue sections of the *Mvh*, *Mili* or *Gasz* mutant adult ovaries, normal folliculogenesis and the corpora lutea were found, indicating that follicle growth and ovulation were

unaffected (Fig. 4D). Notably, even when we combined all three alleles into a triple mutant lacking *Mvh*, *Mili* and *Gasz*, there was no adverse effect on female fertility (supplementary material Table S2).

We assessed meiotic progression by staining E17.5 female genital ridges for synaptonemal complex protein 3 (SYCP3). Synapsis formation was disrupted in a small subset of nuage mutant oocytes, but not in controls (Fig. 4E). Although failure at synapsis leads to meiotic arrest and sterility in the corresponding mutant male mice, we found no effect on overall female fertility. Similarly, others have found mutations in meiotic genes, such as *Pms2* and *Rad21L*, to cause male sterility whereas females remain fertile (Baker et al., 1995; Herrán et al., 2011). In addition, the loss of pachytene, but not pre-pachytene, piRNAs causes male sterility in mice with no effect on retrotransposon expression (Zheng and Wang, 2010), suggesting that these two events are differentially regulated. Hence, it is possible that mouse oocytes only express pre-pachytene piRNAs that control retrotransposon expression, with no apparent meiotic involvement.

Two differences between male and female gametogenesis may also account for this sexual dimorphism. First, female germ cell cysts undergo programmed breakdown, with only ~21% of the oocytes surviving to form primordial follicles (Lei and Spradling, 2013). This process might serve as a form of quality control to remove 'defective' eggs (Pepling and Spradling, 2001). Second, unlike spermatogenesis, which involves continuous meiotic events, oocytes are arrested at meiotic prophase I for a long period of time, possibly allowing time for damage repair.

On the whole, it is becoming apparent that retrotransposon silencing in female gametes involves a timely, coordinated action of multiple mechanisms. DNA methylation in primordial germ cells (PGCs), piRNAs in primordial follicles, the product of meiosis arrest female 1 gene (*Marf1*) in primary follicles (Su et al., 2012), and endogenous small interfering RNAs in mature oocytes (Watanabe et al., 2008), could all act in concert with apolipoprotein B editing complex 3 (APOBEC3) (MacMillan et al., 2013) to prevent transposon expression and/or integration. Enmeshment of these multiple processes appears to be required to suppress endogenous retrotransposon activation and any ensuing genomic instability.

Acknowledgements

We thank B. Cullen (Duke University Medical Center) for IAP-GAG antibodies; T. Kai for experimental discussion; and C. Y. Lim for critical reading of the manuscript.

Funding

This research was funded by A*STAR, Singapore. *Gasz* knockout mice were originally prepared with the support of Eunice Kennedy Shriver NICHD/NIH through cooperative agreement U01-HD060496.

Competing interests statement

The authors declare no competing financial interests.

Author contributions

A.K.L., C.L., T.G.C., D.M.M., D.S. and B.B.K. designed the experiments. A.K.L., C.L., T.G.C., C.W.G.T., Y.T.S., S.B., N.G. and B.B.K. performed the experiments. A.K.L., S.K., M.M.M., S.C. and B.B.K. generated the critical reagents. A.K.L., D.M.M., D.S. and B.B.K. were responsible for manuscript preparation.

Supplementary material

Supplementary material available online at <http://dev.biologists.org/lookup/suppl/doi:10.1242/dev.099184/-/DC1>

References

Aravin, A. A., Sachidanandam, R., Girard, A., Fejes-Toth, K. and Hannon, G. J. (2007). Developmentally regulated piRNA clusters implicate MILI in transposon control. *Science* **316**, 744-747.

Aravin, A. A., van der Heijden, G. W., Castañeda, J., Vagin, V. V., Hannon, G. J. and Bortvin, A. (2009). Cytoplasmic compartmentalization of the fetal piRNA pathway in mice. *PLoS Genet.* **5**, e1000764.

Baker, S. M., Bronner, C. E., Zhang, L., Plug, A. W., Robatzek, M., Warren, G., Elliott, E. A., Yu, J., Ashley, T., Arnheim, N. et al. (1995). Male mice defective in the DNA mismatch repair gene *PMS2* exhibit abnormal chromosome synapsis in meiosis. *Cell* **82**, 309-319.

Brennecke, J., Aravin, A. A., Stark, A., Dus, M., Kellis, M., Sachidanandam, R. and Hannon, G. J. (2007). Discrete small RNA-generating loci as master regulators of transposon activity in *Drosophila*. *Cell* **128**, 1089-1103.

Castrillon, D. H., Quade, B. J., Wang, T. Y., Quigley, C. and Crum, C. P. (2000). The human *VASA* gene is specifically expressed in the germ cell lineage. *Proc. Natl. Acad. Sci. USA* **97**, 9585-9590.

Chuma, S., Hosokawa, M., Kitamura, K., Kasai, S., Fujioka, M., Hiyoshi, M., Takamune, K., Noce, T. and Nakatsuji, N. (2006). Tdrd1/Mtr-1, a tudor-related gene, is essential for male germ-cell differentiation and nuage/germinal granule formation in mice. *Proc. Natl. Acad. Sci. USA* **103**, 15894-15899.

Chuong, E. B., Rumi, M. A. K., Soares, M. J. and Baker, J. C. (2013). Endogenous retroviruses function as species-specific enhancer elements in the placenta. *Nat. Genet.* **45**, 325-329.

Ding, X., Guan, H. and Li, H. (2013). Characterization of a piRNA binding protein Miwi in mouse oocytes. *Theriogenology* **79**, 610-615.e611.

Eddy, E. M. (1976). Germ plasm and the differentiation of the germ cell line. *Int. Rev. Cytol.* **43**, 229-280.

Herrán, Y., Gutiérrez-Caballero, C., Sánchez-Martín, M., Hernández, T., Viera, A., Barbero, J. L., de Álava, E., de Rooij, D. G., Suja, J. A., Llano, E. et al. (2011). The cohesin subunit RAD21L functions in meiotic synapsis and exhibits sexual dimorphism in fertility. *EMBO J.* **30**, 3091-3105.

Kazanian, H. H. Jr (2004). Mobile elements: drivers of genome evolution. *Science* **303**, 1624-1632.

Kuramochi-Miyagawa, S., Kimura, T., Ijiri, T. W., Isobe, T., Asada, N., Fujita, Y., Ikawa, M., Iwai, N., Okabe, M., Deng, W. et al. (2004). Mili, a mammalian member of piwi family gene, is essential for spermatogenesis. *Development* **131**, 839-849.

Kuramochi-Miyagawa, S., Watanabe, T., Gotoh, K., Totoki, Y., Toyoda, A., Ikawa, M., Asada, N., Kojima, K., Yamaguchi, Y., Ijiri, T. W. et al. (2008). DNA methylation of retrotransposon genes is regulated by Piwi family members MILI and MIWI2 in murine fetal testes. *Genes Dev.* **22**, 908-917.

Kuramochi-Miyagawa, S., Watanabe, T., Gotoh, K., Takamatsu, K., Chuma, S., Kojima-Kita, K., Shiromoto, Y., Asada, N., Toyoda, A., Fujiyama, A. et al. (2010). MVH in piRNA processing and gene silencing of retrotransposons. *Genes Dev.* **24**, 887-892.

Lander, E. S., Linton, L. M., Birren, B., Nusbaum, C., Zody, M. C., Baldwin, J., Devon, K., Dewar, K., Doyle, M., FitzHugh, W. et al.; International Human Genome Sequencing Consortium (2001). Initial sequencing and analysis of the human genome. *Nature* **409**, 860-921.

Le Thomas, A., Rogers, A. K., Webster, A., Marinov, G. K., Liao, S. E., Perkins, E. M., Hur, J. K., Aravin, A. A. and Tóth, K. F. (2013). Piwi induces piRNA-guided transcriptional silencing and establishment of a repressive chromatin state. *Genes Dev.* **27**, 390-399.

Lei, L. and Spradling, A. C. (2013). Mouse primordial germ cells produce cysts that partially fragment prior to meiosis. *Development* **140**, 2075-2081.

Lim, A. K. and Kai, T. (2007). Unique germ-line organelle, nuage, functions to repress selfish genetic elements in *Drosophila melanogaster*. *Proc. Natl. Acad. Sci. USA* **104**, 6714-6719.

Lim, A. K., Tao, L. and Kai, T. (2009). piRNAs mediate posttranscriptional retroelement silencing and localization to pi-bodies in the *Drosophila* germline. *J. Cell Biol.* **186**, 333-342.

Lorthongpanich, C., Yang, S.-H., Piotrowska-Nitsche, K., Parnpai, R. and Chan, A. W. S. (2008). Development of single mouse blastomeres into blastocysts, outgrowths and the establishment of embryonic stem cells. *Reproduction* **135**, 805-813.

Ma, L., Buchold, G. M., Greenbaum, M. P., Roy, A., Burns, K. H., Zhu, H., Han, D. Y., Harris, R. A., Coarfa, C., Gunaratne, P. H. et al. (2009). GASZ is essential for male meiosis and suppression of retrotransposon expression in the male germline. *PLoS Genet.* **5**, e1000635.

MacMillan, A. L., Kohli, R. M. and Ross, S. R. (2013). APOBEC3 inhibition of mouse mammary tumor virus infection: the role of cytidine deamination versus inhibition of reverse transcription. *J. Virol.* **87**, 4808-4817.

Mouse Genome Sequencing Consortium, Waterston, R. H., Lindblad-Toh, K., Birney, E., Rogers, J., Abril, J. F., Agarwal, P., Agarwala, R., Ainscough, R., Alexandersson, M. et al. (2002). Initial sequencing and comparative analysis of the mouse genome. *Nature* **420**, 520-562.

Peaston, A. E., Esvikov, A. V., Graber, J. H., de Vries, W. N., Holbrook, A. E., Solter, D. and Knowles, B. B. (2004). Retrotransposons regulate host genes in mouse oocytes and preimplantation embryos. *Dev. Cell* **7**, 597-606.

Pepling, M. E. and Spradling, A. C. (1998). Female mouse germ cells form synchronously dividing cysts. *Development* **125**, 3323-3328.

- Pepling, M. E. and Spradling, A. C. (2001). Mouse ovarian germ cell cysts undergo programmed breakdown to form primordial follicles. *Dev. Biol.* **234**, 339-351.
- Pepling, M. E., Wilhelm, J. E., O'Hara, A. L., Gephardt, G. W. and Spradling, A. C. (2007). Mouse oocytes within germ cell cysts and primordial follicles contain a Balbiani body. *Proc. Natl. Acad. Sci. USA* **104**, 187-192.
- Perrat, P. N., DasGupta, S., Wang, J., Theurkauf, W., Weng, Z., Rosbash, M. and Waddell, S. (2013). Transposition-driven genomic heterogeneity in the *Drosophila* brain. *Science* **340**, 91-95.
- Pillai, R. S. and Chuma, S. (2012). piRNAs and their involvement in male germline development in mice. *Dev. Growth Differ.* **54**, 78-92.
- Rouget, C., Papin, C., Boureux, A., Meunier, A.-C., Franco, B., Robine, N., Lai, E. C., Pelisson, A. and Simonelig, M. (2010). Maternal mRNA deadenylation and decay by the piRNA pathway in the early *Drosophila* embryo. *Nature* **467**, 1128-1132.
- Shoji, M., Tanaka, T., Hosokawa, M., Reuter, M., Stark, A., Kato, Y., Kondoh, G., Okawa, K., Chujo, T., Suzuki, T. et al. (2009). The TDRD9-MIWI2 complex is essential for piRNA-mediated retrotransposon silencing in the mouse male germline. *Dev. Cell* **17**, 775-787.
- Smallwood, S. A. and Kelsey, G. (2012). De novo DNA methylation: a germ cell perspective. *Trends Genet.* **28**, 33-42.
- Su, Y.-Q., Sun, F., Handel, M. A., Schimenti, J. C. and Eppig, J. J. (2012). Meiosis arrest female 1 (MARF1) has nuage-like function in mammalian oocytes. *Proc. Natl. Acad. Sci. USA* **109**, 18653-18660.
- Tanaka, S. S., Toyooka, Y., Akasu, R., Katoh-Fukui, Y., Nakahara, Y., Suzuki, R., Yokoyama, M. and Noce, T. (2000). The mouse homolog of *Drosophila* Vasa is required for the development of male germ cells. *Genes Dev.* **14**, 841-853.
- Watanabe, T., Totoki, Y., Toyoda, A., Kaneda, M., Kuramochi-Miyagawa, S., Obata, Y., Chiba, H., Kohara, Y., Kono, T., Nakano, T. et al. (2008). Endogenous siRNAs from naturally formed dsRNAs regulate transcripts in mouse oocytes. *Nature* **453**, 539-543.
- Yamaguchi, S., Kimura, H., Tada, M., Nakatsuji, N. and Tada, T. (2006). Nanog expression in mouse germ cell development. *Gene Expr. Patterns* **5**, 639-646.
- Yan, W., Rajkovic, A., Viveiros, M. M., Burns, K. H., Eppig, J. J. and Matzuk, M. M. (2002). Identification of Gasz, an evolutionarily conserved gene expressed exclusively in germ cells and encoding a protein with four ankyrin repeats, a sterile-alpha motif, and a basic leucine zipper. *Mol. Endocrinol.* **16**, 1168-1184.
- Zheng, K. and Wang, P. J. (2010). Blockade of pachytene piRNA biogenesis reveals a novel requirement for maintaining post-meiotic germline genome integrity. *PLoS Genet.* **8**, e1003038.

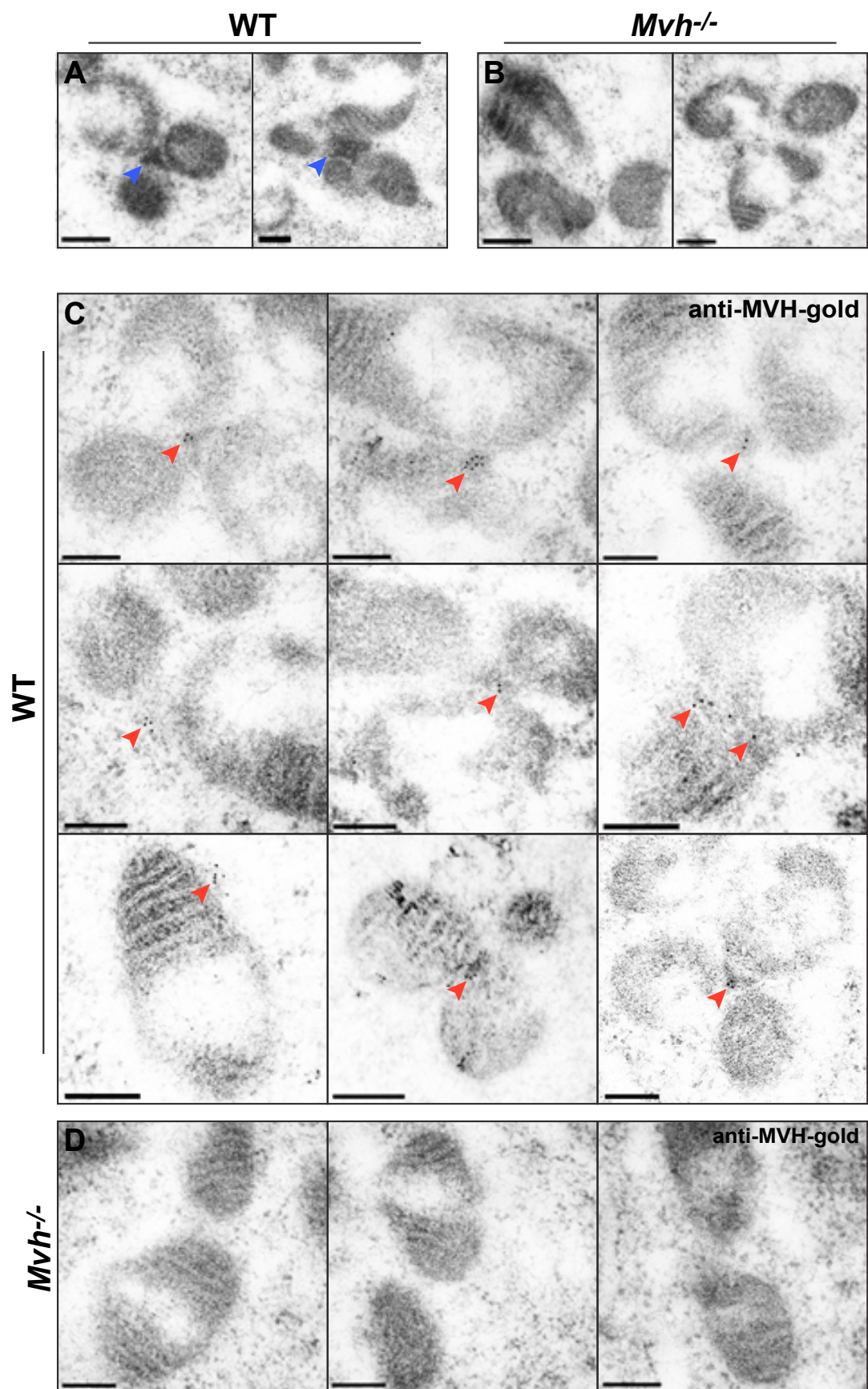


Fig. S1. The electron-dense intermitochondrial cement/nuage is disrupted in *Mvh* mutant ovaries. (A,B) Electron micrographs of intermitochondrial cement/nuage in primordial follicles of P5 wild-type (A) and *Mvh* mutant (B) ovaries. (C,D) Electron micrographs of immuno-gold-labeled MVH in primordial follicles of P5 wild-type (C) and *Mvh* mutant (D) ovaries. Blue and red arrowheads indicate the intermitochondrial cement and MVH-gold labeling, respectively. Scale bars: 200 nm.

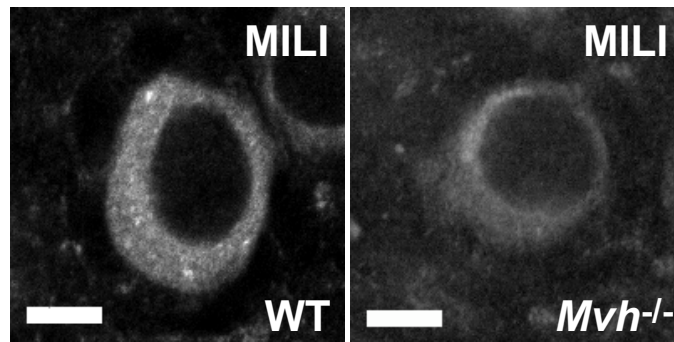


Fig. S2. MILI forms a large aggregate in *Mvh* mutant ovaries. IFA of MILI in P5 ovaries of wild-type and *Mvh* mutants. Scale bar: 10 μ m.

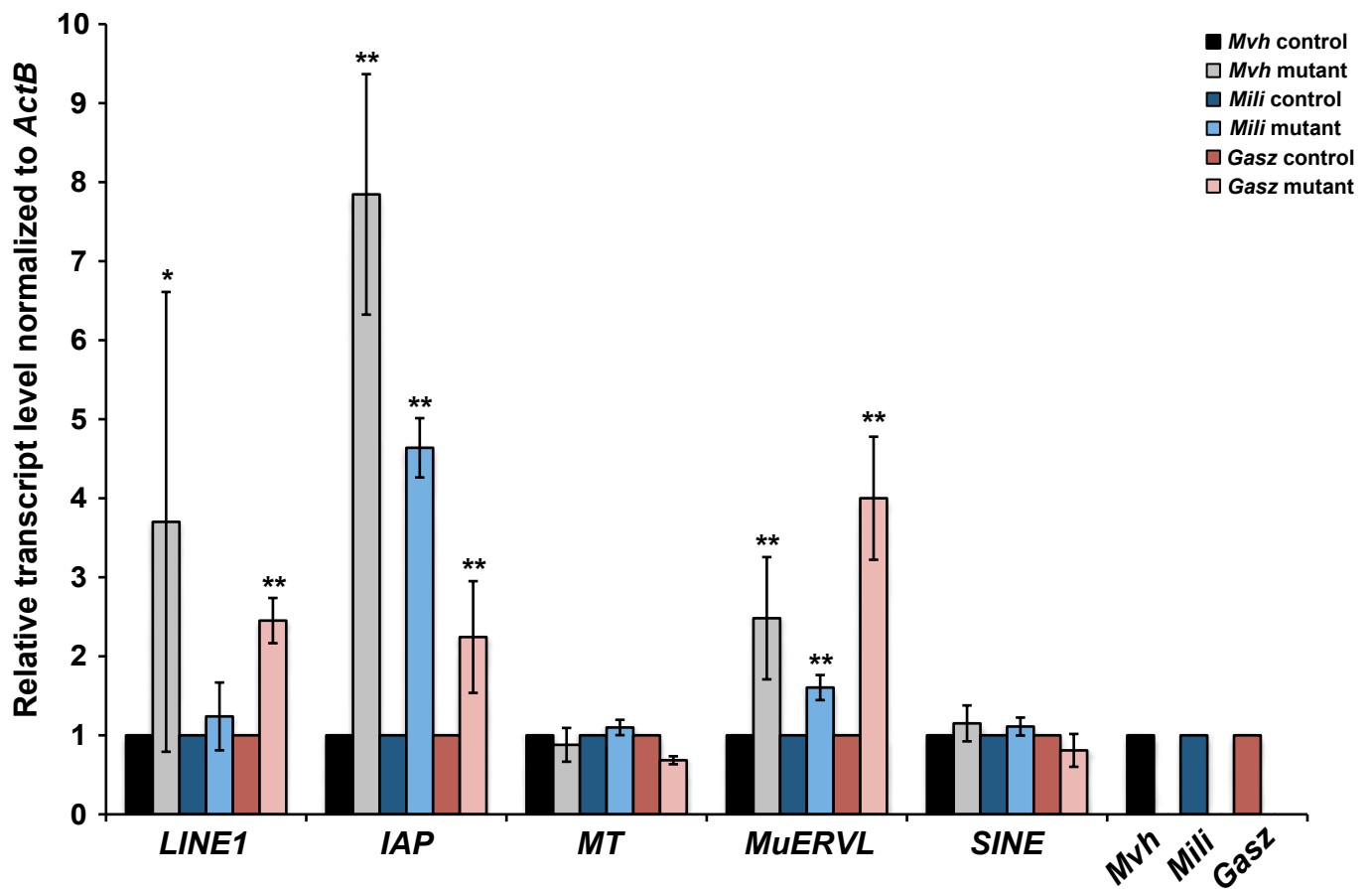


Fig. S3. Some retrotransposons are upregulated in *Mvh*, *Mili* and *Gasz* mutant mature oocytes. qRT-PCR of retrotransposon transcript levels in *Mvh*, *Mili* and *Gasz* mutant MII oocytes. Retrotransposons *LINE1*, *IAP* and *MuERV1*, but not *MT* and *SINE*, are differentially upregulated in the nuage mutant MII oocytes. * $P < 0.05$, ** $P < 0.01$, $n = 3$. Error bars represent s.d.

1 **Table S1. Primer sequences**

Primer name	Sequence
<i>ActB</i> Fw	aaggccaaccgtgaaaagat
<i>ActB</i> Rv	gtggtacgaccagaggcatac
<i>LINE1</i> Fw	ttattaatagtctcccagccaaaaa
<i>LINE1</i> Rv	tgaaggctctgatagaactctgcac
<i>IAP</i> Fw	ttggcagataaggccactaaa
<i>IAP</i> Rv	atttcttcgagcctctaccg
<i>MT</i> Fw	gcattactgggactattgatgct
<i>MT</i> Rv	tcatgctgggtctcttcttaatcac
<i>MuERVL</i> Fw	ggctgctctaccacttggac
<i>MuERVL</i> Rv	tcagccacagacacctcaag
<i>SINE</i> Fw	acgcctttaatcccagcac
<i>SINE</i> Rv	ctggcctcgaactcagaaat
<i>Mvh</i> Fw	tgaaggagggtgaaagcagtg
<i>Mvh</i> Rv	ataatgtgcaaagatggagtcct
<i>Mili</i> Fw	cagctggggacagcaaac
<i>Mili</i> Rv	gaactaccttctcccagcattc
<i>Gasz</i> Fw	gaaagcactgaccactggaga
<i>Gasz</i> Rv	aagaggggtccatccatagc
<i>Dnajc11</i> Fw	gaacacagccagcgacatc
<i>Dnajc11</i> Rv	gattcctgcattagccgaac
<i>Glcc1</i> Fw	gggagcagaaaaacgatcac
<i>Glcc1</i> Rv	gcgttgtagctgttgccctaa
<i>Spin1</i> Fw	gccagtaagaaacatcctcca
<i>Spin1</i> Rv	cttgcttggtcccacactg
<i>5S rRNA</i> Fw	tctacggccataaccacctga
<i>piRNA1</i> Fw	gactctagataccggggttca
<i>piRNA2</i> Fw	tgtctgctactccgtgccta
<i>piRNA3</i> Fw	aagccagtctaatagccacaa
<i>piRNA4</i> Fw	taccaatcccagcaatgcc
<i>Dnajc11 piRNA1</i> Fw	aagaggatgacgcgtgtgctacaaa
<i>Dnajc11 piRNA2</i> Fw	tctggagccaagaggatgacg

2

Table S2. Litter size in triple mutant female mice

	Average litter size (mean \pm s.d.)
Triple mutant 1 (7-month-old)	9.33 \pm 3.67 ($n=6$)
Triple mutant 2 (8-month-old)	8.20 \pm 1.64 ($n=5$)
Triple mutant 3 (7-month-old)	9.00 \pm 2.97 ($n=6$)
Triple mutant 4 (4-month-old)	7.50 \pm 2.12 ($n=2$)

Triple mutant mice were from an outbred genetic background, prior to backcrossing (age at last litter)
 n , number of litters